Influence of bismuth oxide as a sintering aid on the densification of cold sintering of zirconia

Bhootpur, Nikhil; Brouwer, Hans; Tang, Yinglu

DOI
10.1016/j.ceramint.2023.07.207

Publication date
2023

Document Version
Final published version

Published in
Ceramics International

Ceramics International 49 (2023) 33495–33499

Contents lists available at ScienceDirect

Ceramics International

journal homepage: www.elsevier.com/locate/ceramint

Influence of bismuth oxide as a sintering aid on the densification of cold sintering of zirconia

Nikhil Bhootpur, Hans Brouwer, Yinglu Tang *

Techinische Universiteit of Delft, Delft, Netherlands

ARTICLE INFO

Handling Editor: Dr P. Vincenzini

Keywords:
Low temperature (cold) sintering
Sintering aid
Spark plasma sintering
Zirconium hydroxide

ABSTRACT

In the past decades, Zirconia (ZrO_2) has emerged as a promising technical ceramic, both as high temperature structural material and electrolyte for fuel cells, etc. The traditional synthesis of ZrO_2 with spark plasma sintering (SPS) usually requires a sintering temperature as high as 1200 °C. General interest in lowering the sintering temperature to reduce energy consumption and thermal stresses has led to research on two promising routes – cold sintering via temperature-dependent chemical reactivity and sintering aids, which facilitates mass transport and improves densification. Here we combine both by developing a single-step sintering process benefitting from both water vapor through the in-situ conversion of $Zr(OH)_4$ to ZrO_2 and liquid phase Bi_2O_3 as a sintering aid. The resultant ZrO_2 has a relative density above 80% with a sintering temperature as low as 900 °C, significantly higher than that of ZrO_2 without sintering aids, which had a relative density of 54%, both sintered at 50 MPa. The dependence of porosity of sintered samples as a function of sintering pressure (range: 50 MPa–300 MPa) and temperature (range 400 °C–1200 °C) is mapped out as guidance for further material property design. A linear relationship between hardness and relative density was found, with a maximal hardness of 6.6 GPa achieved in samples with 30% porosity. In addition to sintered density, phase stabilization of tetragonal ZrO_2 is enhanced at sintering temperature of 900 °C with water vapor and Bi_2O_3, respectively.

1. Introduction

ZIrconium dioxide (Zirconia) is a functional ceramic which could serve both structural and functional purposes in applications such as in aerospace, automotive, dental, medical, and other industries. In the past, numerous studies [1–5] on traditional spark plasma sintering of zirconium oxides have discovered that 1200 °C is the ideal sintering temperature for Zirconia to achieve a relative density of 80% or higher.

Recent studies have [6–11] explored a novel route of sintering ceramics at temperatures lower than their traditional sintering temperatures called the cold sintering technique by utilizing solvents in the sintering system. Thermodynamically, the liquid phase (various polar solvents, such as water) partially dissolves the surfaces of ceramic particulates, followed by their evaporation upon heating, yielding to a supersaturated solution for precipitation; and kinetically, mass transport is facilitated through enhancing the diffusion of solute ions; also, the liquid phase wets the particle surfaces, hence further benefits particle rearrangement for compaction under pressure [7].

Even though cold sintering process has the advantage of reducing energy required in conventional high temperature sintering processes, it also has many disadvantages. Firstly, the densities of the as-sintered samples are often much lower as compared to the traditional sintering protocols. Additionally, the hardness of the cold-sintered samples are also reported to be lesser than the traditionally sintered samples, which affect their application in many industries. As a result, it is not uncommon practice to add a conventional sintering/annealing step to further density the samples, however, this turns into a two-step sintering process, which not only adds complexity but moreover contradicts the original energy-saving purpose.

Hydroxide precursors of Zirconia could convert into ZrO_2 and water vapor upon heating and were used as starting powders to achieve low-temperature sintering by Elissalde et al. [13]. A relative density of 70–80% could be achieved after 10 min dwelling at 350 °C and 600 MPa. To promote sintering of ceramic powders with high melting temperatures, sintering aids are often used [14–18]. One of the reasons they work is due to liquid phase sintering [15]. The sintering aid melts at a certain temperature and becomes liquid that fills in between the solid powder particles. With a nonzero solubility of solid powder in the liquid

* Corresponding author.
E-mail address: y.tang-5@tudelft.nl (Y. Tang).

https://doi.org/10.1016/j.ceramint.2023.07.207
Received 1 June 2023; Received in revised form 11 July 2023; Accepted 24 July 2023
Available online 1 August 2023

phase, the mass transport can be enhanced through diffusion of the solutes and the particle edges can also be wet to facilitate particle rearrangement, both of which is similar to the principles of cold sintering. However, in contrast to cold sintering where the solvent will eventually evaporate and leave the system, sintering aids will remain in the system, most likely in solid solution form. This alters the stoichiometry of the original sintering powders and could affect various properties, such as thermal and mechanical properties [17,18].

Compared to other various sintering aids, bismuth oxide has a melting temperature at 817 °*C* which is lower than the usual sintering temperatures of ZrO_2 (higher than 1200 °*C*) but also still high enough to promote decent sintering. Moreover, the solubility of ZrO_2 in bismuth oxide was found to be between 2 and 10 mol% between 800 °*C* and 900 °*C* [19], which is promising to induce liquid phase sintering. While the solubility of Bi_2O_3 in ZrO_2 is preferably to be small so the liquid phase wouldn't be transient, unfortunately this data remain lacking in literature despite the fact that Bi_2O_3 was previously used as a tetragonal phase stabilizer in Zirconia systems at low temperatures by Gulino et al. [12]. One of our goals in this study is thus to investigate whether Bi_2O_3 can be an effective liquid phase sintering aid for ZrO_2.

In this study, we combine both advantages from cold sintering effect provided by the in-situ conversion of $Zr(OH)_4$ to ZrO_2 and H_2O at 400 °C and sintering aided by Bi_2O_3 in the temperature range of 817 °C–900 °C, effectively achieving a density of 87% with a sintering temperature as low as 900 °C in a 'single sintering step'. Different piston pressures (50 MPa, 150 MPa, 300 MPa) and different weight percentages of Bi_2O_3 (5 wt%, 10 wt%, 15 wt%) in Zirconium dioxide and Zirconium hydroxide systems were employed. The resultant density and hardness values were tabulated to assist in further material property design. Also, phase composition and microstructural analysis were performed.

2. Methods

2.1. Spark plasma sintering

Zirconium (IV) hydroxide (97%, powder, density-3.25 g/cc) from Sigma-Aldrich, Zirconium (IV) oxide (99%, powder density-5.89 g/cc), Bismuth (III) oxide (99.8%, powder, size: 90–210 nm, density-8.937 g/cc), both from Aldrich Chemistry were used as the starting powders. Spark plasma sintering of these ceramic powders was performed using the FCT Systeme Gmbh SPS machine at the Delft University of Technology. The powder systems (a) Pure Zirconium hydroxide, (b) pure Zirconium oxide, (c) Zirconium hydroxide – Bi_2O_3 sintering aid, and (d) Zirconium oxide – Bi_2O_3 sintering aid were all sintered under vacuum are hereafter referred to as (a), (b), (c), and (d) respectively. The powder systems (a) and (b) were ground using mortar and pestle before filling them in the die for sintering, whereas powder systems (c) and (d) were prepared by mixing them in the required ratio in a planetary ball mill with 2-propanol as a disperser. Since these powders are insoluble in alkalis and water, no change in the composition due to the wet mixing is expected. The 'ball mass: powder mass' ratio was always maintained as 4:1. They were wet-mixed for 3 h at a 300-rpm rotation speed, and the slurry was later dried overnight in the fume hood under atmosphere. These powders were also ground using mortar and pestle before filling them in the die prior to sintering.

Dies made of either (i) Graphite (maximum mechanical loading-50 Mpa) or (ii) Stainless steel (maximum mechanical loading-150 Mpa), or (iii) Tungsten carbide-Cobalt (maximum mechanical loading-300 Mpa) were used depending on the dwell piston pressure of the sintering cycle. The inner surface of the hollow cylindrical die was covered with thin Graphite foils to ensure uniform electric current conduction throughout the die. The powders were then weighed and filled in the die with thin Graphite discs at both end surfaces for uniform electrical conduction. The die assembly was then pressed under a hydraulic press under 1-ton force (10 kN) to prepare the cylindrical green body. The die was placed in the SPS machine and sintered with a uniform temperature ramp of 50 °C/min to the dwell temperature. The dwell temperature is kept constant for 10 min before free cooling the system back to ambient temperature. The mechanical loadings were also ramped up simultaneously with the temperature to reach the dwell piston pressure, kept constant until the end of the cycle, even while cooling the system. The whole process was performed under vacuum. The same cycle was followed for all the SPS experiments, as depicted in Fig. 1.

2.2. Material characterisation

Zirconium hydroxide powders were analyzed for their thermal behavior using Thermogravimetric analysis and Differential Scanning Calorimetry (DSC). These tests were also helpful to confirm the conversion to Zirconium oxide. For the TGA, the powders were heated from ambient temperature to 900 °C with a heating rate of 50 °C/min to mimic the sintering cycle used in the experiments. For the DSC, the powders were heated from ambient temperature up to 600 °C and back to ambient temperature with a heating and cooling rate of 5 °C/min to closely measure heat flow at each temperature step.

The microstructural analysis of as-sintered pellets after the SPS cycle was analyzed performed with a JEOL JSM7000F Scanning Electron Microscope (SEM). The extent of sintering in the sample was examined by observing the microstructure in comparison to relative density data. Energy Dispersive Spectroscopy (EDS) was performed on the same samples at random spots to verify the conversion to Zirconium oxide via the measured stoichiometry of Zr:O.

X-ray Diffraction (XRD) spectroscopy using Rigaku MiniFlex 600 was performed to measure the phase composition, especially different phases of Zirconia. Cu-α X-rays were used with a set diffraction angle range of $2\Theta = 10°–80°$.

2.3. Density and hardness measurements

Geometrical dimensions of the as-sintered pellets were used to calculate the density of the pellets instead of Archimedes' method since the pellets have large porosity and are prone to property alteration due to solvent absorption. Relative densities were measured with respect to the density of tetragonal Zirconia, i.e., 6.10 g/cc [X], on which the aerospace application of the ceramic is based. Since the density of tetragonal ZrO_2 is the highest among all its different phase forms while the sintered sample often contain other ZrO_2 phases such as monoclinic (5.68 g/cm^3) and cubic phase (6.09 g/cm^3), the calculated density $\left(\frac{\text{Density of pellet (g/cc)}}{6.10\ \text{g/cc}} * 100\right)$ gives a conservative lowest estimation. It was calculated using the formula

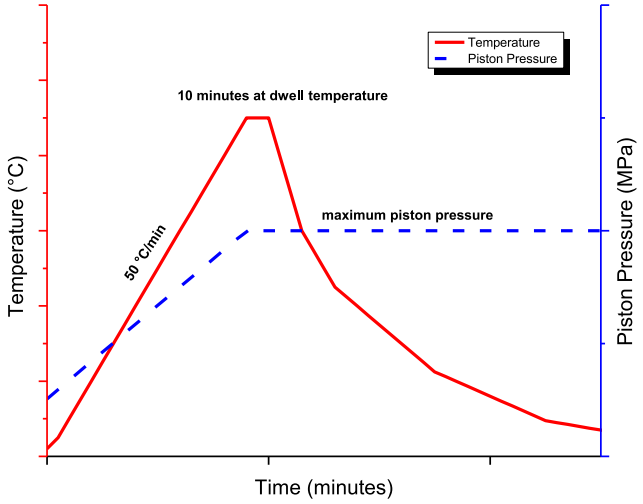

Fig. 1. SPS Pressure-Temperature profile followed for all the experiments.

The hardness of the as-sintered pellets was measured using the Leitz Durimet micro Vickers hardness testing machine. A counterweight of 500 P (0.5 Kg = 4.905 N) for around 15 s was applied to indent the sample surface. A magnified image of the indentation aided the measurement of the diagonals of the intender. The Vickers hardness number was calculated using the formula $HV = \frac{0.1891 * F}{d^2}$ where; HV is Vickers hardness (N/mm^2), F is the applied force = 4.905 N, and d is the average length of the diagonals (mm).

3. Results and discussion

3.1. Conversion to zirconium oxide

The decomposition of $Zr(OH)_4$ to ZrO_2 is accompanied by dehydration from the system.

$$Zr(OH)_4 \rightarrow ZrO_2 + 2H_2O\uparrow \quad (1)$$

Since water is the by-product that will be released from the hydroxide powders during the reaction, the ideal mass loss on the complete conversion of $Zr(OH)_4$ to ZrO_2 is calculated as follows,

The molecular mass of Zr(OH)4 = 159.22 g/mol

The molecular mass of ZrO2 = 123.22 g/mol

The molecular mass of H2O = 18 g/mol

$$Zr(OH)_4 \rightarrow ZrO_2+2H_2O\uparrow \quad (2)$$

The ideal mass loss % for the complete reaction would then be, 36.00/159.22*100 = 22.61%.

It can also be seen from the TGA analysis with 50 °C/min heating ramp up to 900 °C shown in Fig. 2 that there is a slope change at around 200 °C, moreover, at beyond 400 °C, the conversion saturates. The mass loss at saturation (21.3%) deviates reasonably small (5.8%) from the calculated theoretical value (22.61%), signifying that the conversion to oxides is indeed accompanied by the dehydration of the precursor hydroxide powders.

The DSC curve from Fig. 3 shows an endothermic heat change around between 100 °C and 200 °C. The peak at 185 °C can be attributed to the initial dehydration of the hydroxide powders after the boiling point of water is reached. The curve undergoes a significant shift at 403 °C, where it reaches an exothermic peak corresponding to the crystallization of amorphous to crystalline zirconium oxide, which again confirms the $Zr(OH)_4$ to ZrO_2 conversion.

Mass spectrometry embedded with the DSC machine measured the outlet gas composition from the pure $Zr(OH)_4$ system. In Fig. 4, it is shown that water liberation from the system was detected beginning from 100 °C, which reached the maximum at 185 °C and finished at about 200 °C. This agrees well with the DSC measurement. At temperatures higher than 200 °C, water detection slowly decreased to $2.0 * 10^{-8}$ g (10 mg – total sample weight), which corresponds well to the slope change in the TGA analysis. Another small peak of water detection occurs at 405 °C, which agrees well with DSC peak at 403 °C and could be explained by different amount of water crystallization in amorphous and crystalline ZrO_2. The water detection approaches towards zero at temperatures above 405 °C and during cooling stage as well, which supports the saturation observation found in TGA analysis (Fig. 2).

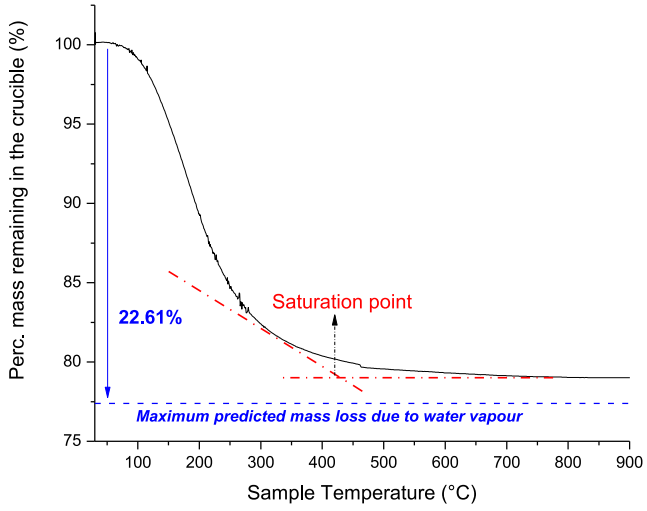

Fig. 2. Thermogravimetric analysis of the pure $Zr(OH)_4$ powders.

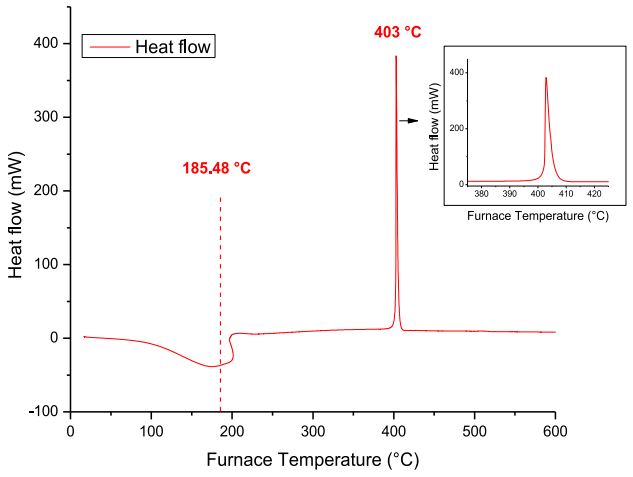

Fig. 3. Differential scanning calorimetry of the pure $Zr(OH)_4$ powders.

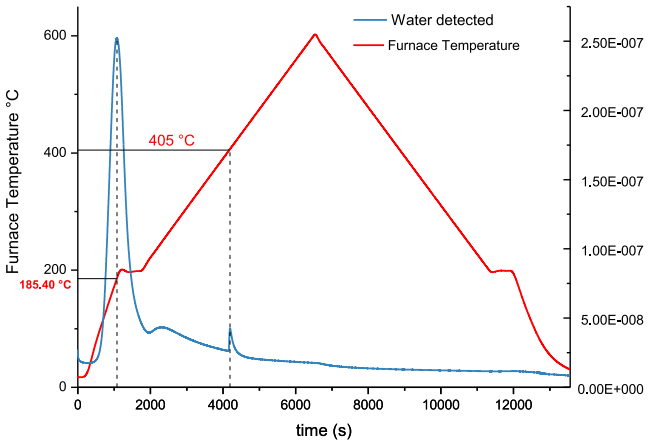

Fig. 4. Mass spectrometry associated with the temperature behavior of $Zr(OH)_4$.

3.2. Influence of cold sintering due to $Zr(OH)_4$ to ZrO_2 conversion on densification of ZrO_2

It can be seen from Fig. 5 that for pure ZrO_2 systems, temperature and pressure do not influence sintering as evident from their relative densities, which remain in the similar range even with the increase in temperature (from 400 °C to 900 °C) and pressure (from 50 MPa to 300 MPa). Whereas, the pure $Zr(OH)_4$ system samples exhibit a significant enhancement in the relative density values with both the increasing temperature and the increasing piston pressure. A combination of the effect of cold sintering process and high pressure assisted locking of water vapor within the sintering body and rearrangement of the powder

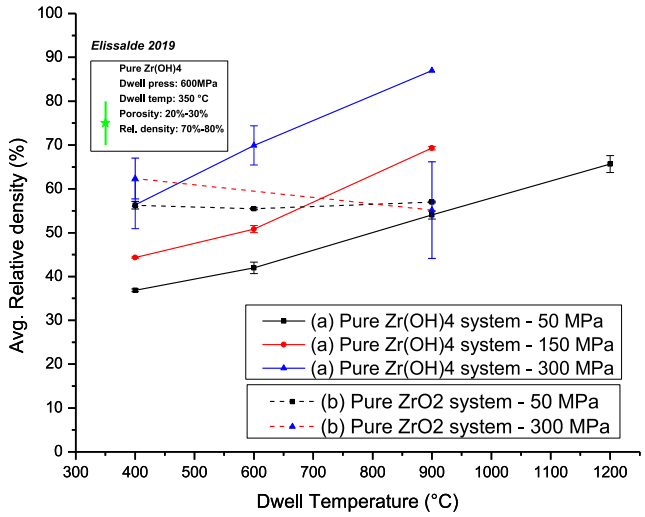

Fig. 5. Influence of sintering temperature and pressure on relative density for cold sintered $Zr(OH)_4$ and ZrO_2.

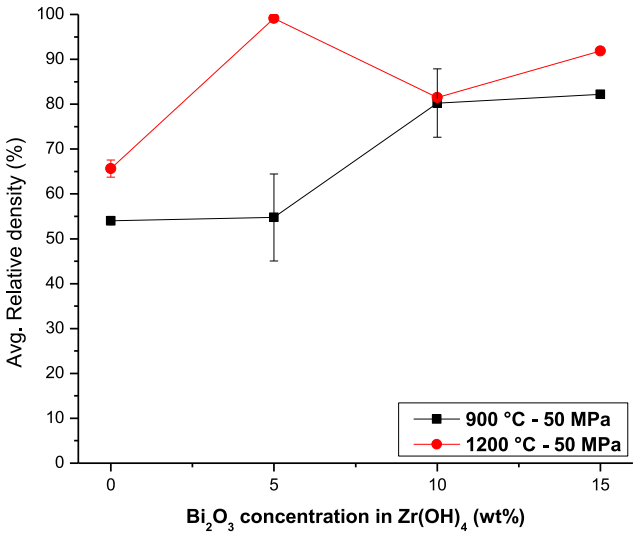

Fig. 7. Influence of sintering aid-Bi_2O_3 on the relative density.

particles is likely the reason for this distinctive contrast in sintering behavior between $Zr(OH)_4$ and ZrO_2.

SEM images of the polished surface of ZrO_2 at different magnifications are shown in Fig. 6. The sample was prepared from $Zr(OH)_4$ and sintered at 900 °*C* and 300 MPa, with a measured relative density of 90%. The white area in Fig. 6a is pore and the grey area is ZrO_2.

3.3. *Influence of sintering aid- Bi_2O_3 on densification of $Zr(OH)_4$*

The phase diagram [19] of the Bi_2O_3–ZrO_2 system denotes that at small concentrations of ZrO_2, Bismuth oxide exists as either α-Bi_2O_3 (monoclinic) or δ-Bi_2O_3 (cubic) or in liquid phase [20] depending on the temperature. In the sintering temperature range we are exploring (400 °C–900 °C), these is reasonable solubility of ZrO_2 in Bi_2O_3, which fulfills one of the most important prerequisites of liquid phase sintering. The effect of these Bi_2O_3 phases on the sintering of Zirconia is explored in this section.

Fig. 7 shows the influence of sintering aid – Bi_2O_3 on the relative densities of the corresponding samples. It is observed that at the same piston pressure of 50 MPa and dwell temperature of 900 °C, the addition of Bi_2O_3 increased the relative density by 25–30% when the composition was, either equal to more than 10 wt% Bi_2O_3. However, at 1200 °C, the 5 wt% (c) sample increased the relative density by almost 35%, whereas the 10 wt% and 15 wt% (c) samples increased the relative densities by 15% and 25% respectively. The 5 wt% (c) samples show higher densities than the 10 wt% (c) and 15 wt% (c) samples The lattice changes associated with phase change of the monoclinic Zirconia into tetragonal Zirconia around 1200 °C, influencing the solubility of bismuth oxide in ZrO_2, can be considered as a reason for this phenomenon Further experiments of solubility study are needed to clarity, given no existing phase diagram data on the ZrO_2-rich end.

3.4. *Influence of sintering conditions (temperature and pressure) and sintering aid-Bi_2O_3 on hardness*

The surface hardness is another measure to indicate the extent of sintering in bulk. Fig. 8 shows the hardness dependency upon temperature, pressure, and addition of Bi_2O_3. For system (a) samples, the hardness increases with increasing temperature and piston pressure in line with the increasing densities of the samples. The decrease of porosities associated with increased densities is responsible for such behavior. Pure $Zr(OH)_4$ sample sintered at 300 MPa–600 °C dwell conditions had a similar hardness value as the one from the samples tested by Elissalde et al. [13] (3.805 GPa) with sintering dwell condition 350 °C–600 MPa. Also, the hardness of the 10 wt% Bi_2O_3–$Zr(OH)_4$ sample (6.59 GPa) sintered at 900 °C–50 MPa piston pressures surpassed this value from the literature, showing prospects of tuning mechanical properties by Bi_2O_3 doping.

3.5. *Phase changes*

Literature [21] found that the Zirconia's tetragonal phase reflections are observed at around 30.25°, and the monoclinic reflections at around 28.20° and 31.47°.

Fig. 9 shows the XRD spectrum comparison between system (a) sample and system (c) sample sintered at the same dwell conditions of

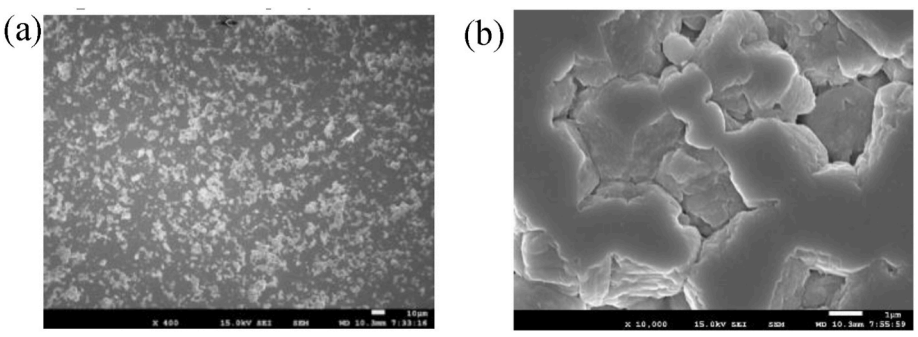

Fig. 6. SEM images of ZrO_2 sintered from Zr(OH)4 at 900 °*C* and 300 MPa.

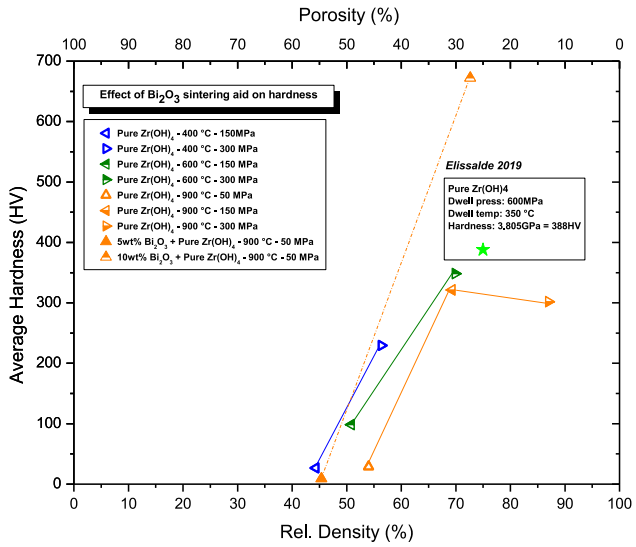

Fig. 8. Influence of piston pressure and sintering aid-Bi2O3 on the hardness values.

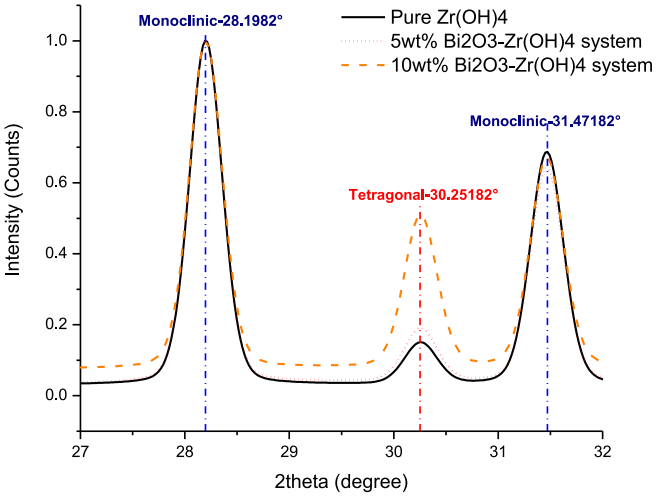

Fig. 9. XRD plots of sintered pure $Zr(OH)_4$, sintered 5 wt% and 10 wt% Bi_2O_3–$Zr(OH)_4$ system at 900 °C, 50 MPa.

50 MPa and 900 °C dwell temperatures. The sintering aid Bi_2O_3 in the starting powders also enhanced the tetragonal phases in the sintered Zirconia system. The 10 wt% Bi_2O_3 system had a higher tetragonal phase stabilization effect than the 5 wt% Bi_2O_3 system.

4. Conclusion

The in-situ liberation of water vapor from the precursors Zirconium hydroxide powders along with the increased piston pressure enhanced the relative densities and hardness of the as-sintered samples. The 10 wt % Bi_2O_3–$Zr(OH)_4$ system sintered at 900 °C–50 MPa dwell conditions had the highest hardness of value of 6.6 GPa, whereas the 5 wt% Bi_2O_3–$Zr(OH)_4$ system had the highest density among all the samples reaching around 99% relative density. The 10 wt% Bi_2O_3–$Zr(OH)_4$ systems also stabilized the tetragonal phase of Zirconia in the sintered samples better than the 5 wt% Bi_2O_3–$Zr(OH)_4$ systems.

Declaration of competing interest

The authors declare that they have no known competing financial interests or personal relationships that could have appeared to influence the work reported in this paper

Acknowledgement

The authors would like to acknowledge Professor S. van der Zwaag for discussions during the project. The authors would like to acknowledge department of aerospace structures and materials (ASM) at TU Delft for funding the research, and department of materials science (3mE) at TU Delft for support of facility usage.

References

[1] O. Guillon, et al., Field-assisted sintering technology/spark plasma sintering: mechanisms, materials, and technology developments, Adv. Eng. Mater. 16 (7) (2014) 830–849, https://doi.org/10.1002/adem.201300409.
[2] E.A. Olevsky, W.L. Bradbury, C.D. Haines, D.G. Martin, D. Kapoor, Fundamental 59 aspects of spark plasma sintering: I. Experimental analysis of scalability, J. Am. Ceram. Soc. 95 (8) (2012) 2406–2413, https://doi.org/10.1111/j.1551-2916.2012.05203.x.
[3] A. Fregeac, F. Ansart, S. Selezneff, C. Estournès, Relationship between mechanical properties and microstructure of yttria stabilized zirconia ceramics densified by spark plasma sintering, Ceram. Int. 45 (17) (2019) 23740–23749, https://doi.org/10.1016/j.ceramint.2019.08.090.
[4] M. Biesuz, V.M. Sglavo, Flash sintering of ceramics, J. Eur. Ceram. Soc. 39 (2) (2019) 115–143, https://doi.org/10.1016/j.jeurceramsoc.2018.08.048.
[5] G. Lee, et al., Effect of electric current on densification behavior of conductive ceramic powders consolidated by spark plasma sintering, Acta Mater. 144 (2018) 524–533, https://doi.org/10.1016/j.actamat.2017.11.010.
[6] H. Guo, A. Baker, J. Guo, C.A. Randall, Protocol for ultralow-temperature ceramic sintering: an integration of nanotechnology and the cold sintering process, ACS Nano 10 (11) (2016) 10606–10614, https://doi.org/10.1021/acsnano.6b03800.
[7] H. Guo, A. Baker, J. Guo, C.A. Randall, Cold sintering process: a novel technique for low-temperature ceramic processing of ferroelectrics, J. Am. Ceram. Soc. 99 (11) (2016) 3489–3507, https://doi.org/10.1111/jace.14554.
[8] H. Guo, J. Guo, A. Baker, C.A. Randall, Cold sintering process for ZrO2-based ceramics: significantly enhanced densification evolution in yttria-doped ZrO_2, J. Am. Ceram. Soc. 100 (2) (2017) 491–495, https://doi.org/10.1111/jace.14593.
[9] J.-P. Maria, et al., Cold sintering: current status and prospects, J. Mater. Res. 32 (17) (2017) 3205–3218, https://doi.org/10.1557/jmr.2017.262.
[10] T. Hérisson de Beauvoir, F. Molinari, U.C. Chung-Seu, D. Michau, D. Denux, M. Josse, Densification of $MnSO_4$ ceramics by Cool-SPS: evidences for a complex sintering mechanism and magnetoelectric coupling, J. Eur. Ceram. Soc. 38 (11) (2018) 3867–3874, https://doi.org/10.1016/j.jeurceramsoc.2018.04.005.
[11] T. Herisson de Beauvoir, et al., Cool-SPS stabilization and sintering of thermally fragile, potentially magnetoelectric, NH4FeP2O7, Ceram. Int. 45 (7, Part B) (2019) 9674–9678, https://doi.org/10.1016/j.ceramint.2018.12.103.
[12] A. Gulino, S. La Delfa, I. Fragalà, R.G. Egdell, Low-temperature stabilization of tetragonal zirconia by bismuth, Chem. Mater. 8 (6) (1996) 1287–1291, https://doi.org/10.1021/cm950558j.
[13] C. Elissalde, et al., Single-step sintering of zirconia ceramics using hydroxide precursors and Spark Plasma Sintering below 400 °C, Scripta Mater. 168 (2019) 134–138, https://doi.org/10.1016/j.scriptamat.2019.04.037.
[14] Y. Dong, et al., A novel way to fabricate highly porous fibrous YSZ ceramics with improved thermal and mechanical properties, J. Eur. Ceram. Soc. 32 (2012) 2213–2218, https://doi.org/10.1016/j.jeurceramsoc.2012.03.016.
[15] Raquel De Oro Calderon, Christian Gierl-Mayer, Herbert Danninger, Fundamentals of Sintering: Liquid Phase Sintering, 2021, https://doi.org/10.1016/B978-0-12-819726-4.00127-7.
[16] M. Mallik, et al., Effect of SiC content, additives and process parameters on densification and structure–property relations of pressureless sintered ZrB_2–SiC composites, Ceram. Int. 39 (2013) 2915–2932, https://doi.org/10.1016/j.ceramint.2012.09.066.
[17] L. Silvestroni, et al., Effects of $MoSi_2$ additions on the properties of Hf– and Zr–B_2 composites produced by pressureless sintering, Scripta Mater. 57 (2007) 165–168, https://doi.org/10.1016/j.scriptamat.2007.02.040.
[18] D. Sciti, et al., Properties of a pressureless-sintered ZrB_2–$MoSi_2$ ceramic composite, J. Am. Ceram. Soc. 89 (2006) 2320–2322, https://doi.org/10.1111/j.1551-2916.2006.00999.x.
[19] T. Takamori, M.W. Shafer, Phase transformation kinetics in the system bismuth oxide-zirconia, J. Am. Ceram. Soc. 73 (1990) 1453–1455, https://doi.org/10.1111/j.1151-2916.1990.tb05227.x.
[20] M. Weber, M. Schlesinger, M. Walther, D. Zahn, C.A. Schalley, M. Mehring, Investigations on the growth of bismuth oxido clusters and the nucleation to give metastable bismuth oxide modifications, Z. für Kristallogr. - Cryst. Mater. 232 (1–3) (2016) 185–207, https://doi.org/10.1515/zkri-2016-1970.
[21] H.T. Rijnten, Zirconia, Tudelft.nl, 1971, http://resolver.tudelft.nl/uuid:dc3174d3-79bb-4730-961a-5d12d960b390.